Final Report: NASA SENH99-0186-0162

And Progress For the Period: 4/15/03-4/14/04

KARHUNEN-LOEVE ANALYSIS OF SCIGN GPS DATA

Principal Investigators:

John B. Rundle
Departments of Geology
and Cooperative Institute for Research in Environmental Sciences
University of Colorado
Boulder, CO 80309
(303) 492 - 1143

Kristy Tiampo
Cooperative Institute for Research in Environmental Sciences
University of Colorado
Boulder, CO 80309

Co-Investigator:

Susanna Gross, Co-Investigator
Cooperative Institute for Research in Environmental Sciences
University of Colorado
Boulder, CO 80309

1. Introduction:

During the final year of this project, we made substantial progress on the proposed work. Specifically, we have continued the horizontal and vertical Karhunen-Loeve (KL) analysis of SCIGN data and implemented the study of a number of particular modes. In particular, we studied the spatial and temporal interactions of these modes in an effort to better understand and model the source of each signal.

2. Progress

Initial work focused on the acquisition of currently available SCIGN GPS data preprocessed by JPL, via ftp, for the more than 125 sites in the current network. The available data was differentiated into two classes, that originally processed prior to 1998, and that processed subsequent to 1998. A later data set provided by JPL, subjected to advanced preprocessing, titled SCIGN 3.0, was acquired for comparison and analysis. Finally, the data was segregated into various spatial subsets.

For each of the existing SCIGN stations, approximately 200 at this time, various strain or deformation time series were identified, and a Karhunen-Loeve expansion (KLE) was performed on the vertical data. At the right is shown the first KL mode for the vertical data in the LA basin. The spatial mode, top, outlines the correlations in the data, where blue is correlated with blue, and red is correlated with red. This mode corresponds to the groundwater changes identified via geodetic means by both Bawden et al., 2001 and Watson et al., 2002. The time series associated with

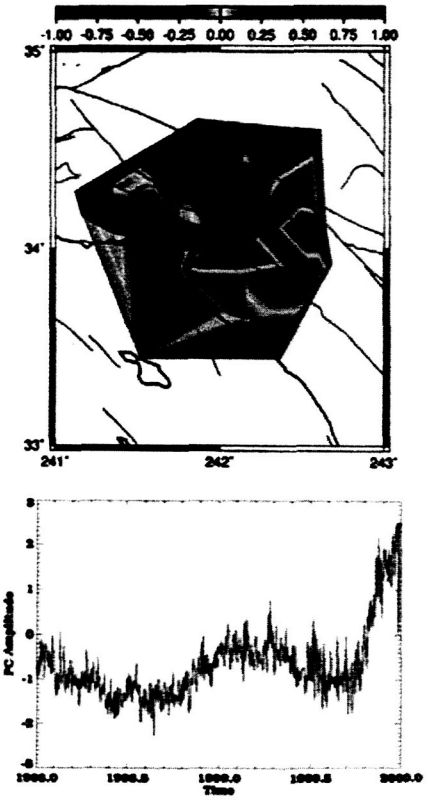

this mode displays the distinct seasonal signal one would expect to see in a groundwater phenomena.

KL mode four for the horizontal deformation, calculated from what is called SCIGN 2.0, 1998-2000, is shown below. The arrows here detail the spatial correlations in the latitude-longitude. The horizontal motion from this mode is centered in the aftershock region of the Northridge earthquake of 1994, suggesting that it is either the direct result of a Northridge aftershock, or a slower temporal signal such as viscoelastic deformation. The associated temporal signal suggests the latter; modeling is currently underway to determine the appropriate source. Note the jump in the time series associate with the Hector Mine event of 1999, which is visible to a greater extent in the decomposition of the entire network, but not detectable over the noise in the vertical LA Basin signal, above, demonstrating the ability of this technique to isolate small signals.

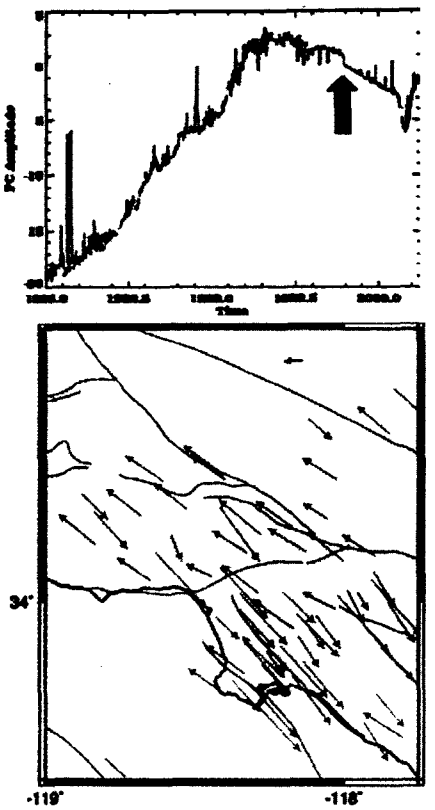

The next series of figures corresponds to the first vertical mode for the entire southern California region for 1995-1998. Here the entire region is correlated, moving together with the temporal pattern shown at the bottom. This seasonal signal is not the simple groundwater motion related to rainfall, snowmelt and drought, but is a complicated mixture of a variety of hydrologic and atmospheric causes, as can be seen in the associated time series.

In the subsequent figure is shown a first attempt to characterize the temporal signal using a model for thermoelastic strain from Ben-Zion and Leary, 1996. While a portion of the signal might correspond to this mechanism, it is second order in both

magnitude and phase. As a result, a comparison with atmospheric pressure was undertaken, as shown on page five.

Atmospheric pressure and precipitation, next page, provide a better explanation of the temporal signal for the mode at the right. The vertical deformation is shown at the top for station CLAR, the middle graph shows the atmospheric pressure, and at the bottom is plotted local precipitation. The atmospheric pressure highs correspond to

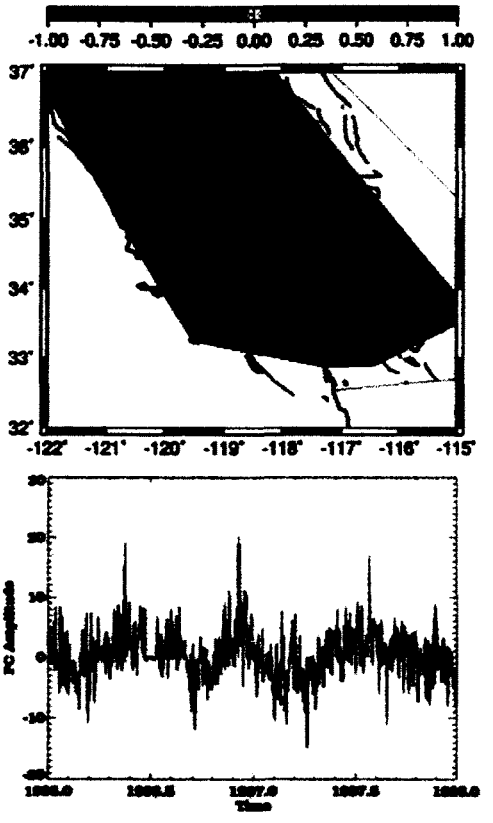

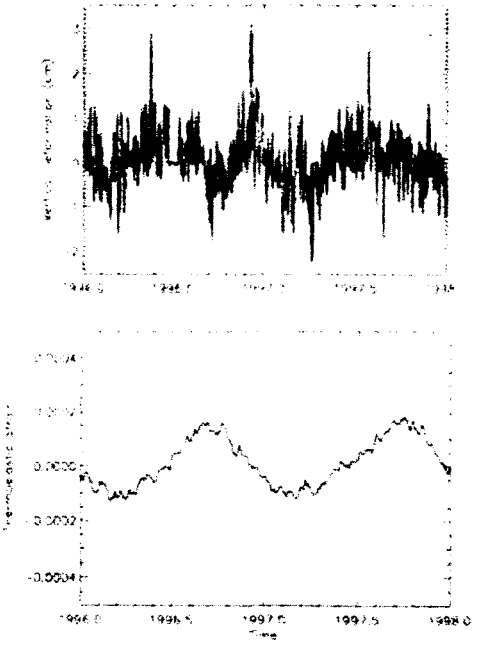

lows in the deformation signal, while significant highs in the deformation lag precipitation by a few months, modulated by highs and lows in the pressure.

Using the elastic fault patch model for southern California, developed in association with this and other work, we have begun testing a new mapping of strain into the underlying stress field.

While the underlying variables of the fault system, in particular the stress field, are inherently unobservable, the surface data is observable. Our goal is to process surface data through a mathematical mapping so that the resulting processed data would resemble the failure stress on each

fault. If the earthquake cycle corresponds to an increase in the local Coulomb Failure Function (CFF) through time as a result of plate tectonic forcing, culminating in an earthquake,

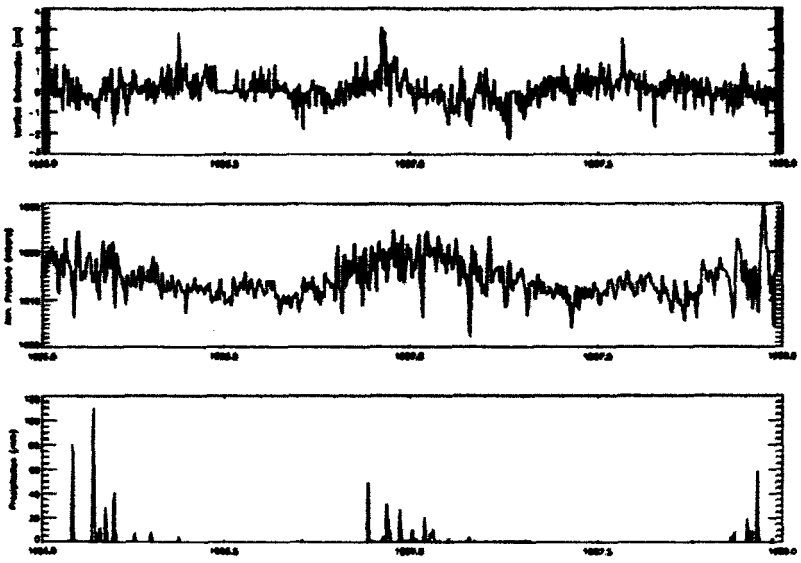

followed by a return to low CFF values, then what we want to do is design a mapping that translates surface measurements to underlying CFF values.

If the earthquake cycle corresponds to an increase in the local Coulomb Failure Function (CFF) through time as a result of plate tectonic forcing, culminating in an earthquake, followed by a return to low CFF values, then what we want to do is design a mapping that translates surface measurements to underlying CFF values. Note, again, that in nature the fault friction strength, as well as the CFF, is inherently unobservable. The interactions among faults and fault segments within an active fault system produce strong space-time correlations in seismic activity and deformation fields along the various faults. While the transfer of elastic stresses using Coulomb failure functions provides a snapshot of the direct effect of one fault upon other smaller ones in the vicinity, it does not measure the time-development of the space-time correlations and patterns that clearly develop in the various data sets as a result of continued dynamical processes through time. The Karhunen-Loeve methodology provides illumination into the stress interactions on the fault network via analysis of the surface deformation.

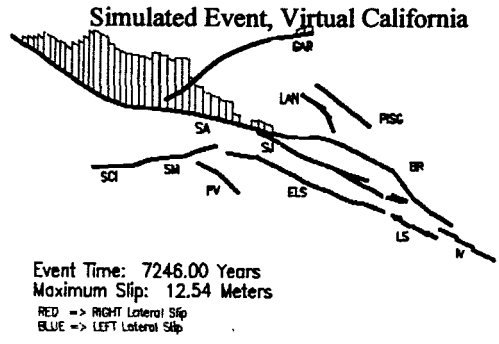

If the CFF is inherently unobservable, the surface data is observable. The figure below is a plot of observable data from a computer simulation of southern California. Both simulated GPS observations and InSAR observations are shown.

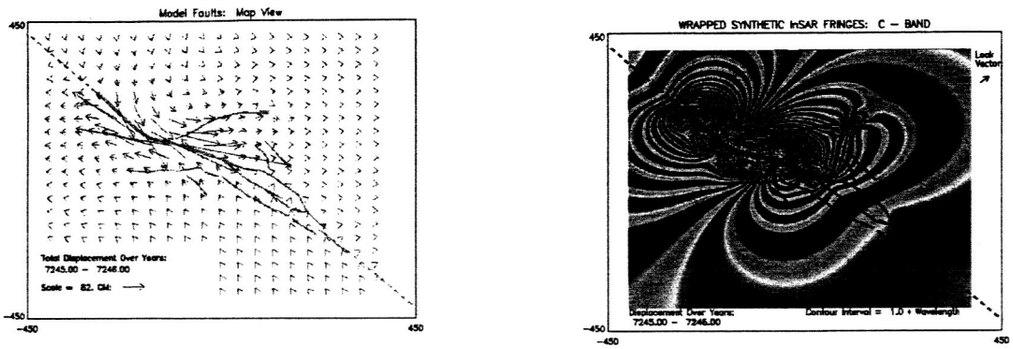

Here we detail a mapping for this surface change into the fault system stress called the "Local Ginzburg Criterion" (LGC) after a somewhat similar method of analysis in the theory of critical phenomena (Ma, 1976). The method consists of defining a normalized, squared, time dependent strain rate for each fault so that all locations can be treated as having the same strain rate statistics.

In the theory of critical phenomena in complex, interacting, nonlinear systems, sudden changes in the dynamical state of the system are usually preceded by large fluctuations in the order parameter. For earthquake fault systems, the order parameter is the slip deficit on a fault, fluctuations of which correspond to fluctuations in strain rate along the fault. The Ginzburg Criterion (GC) is defined to be the variance in the order parameter divided by the square of the mean. When this parameter becomes large, of the order of 10% or more, sudden changes in the order parameter of the system are imminent.

We therefore defined a similar quantity, a fluctuation metric, for each earthquake fault segment as a function of time. The LGC is the surface shear strain rate at time t and position x divided by the time average of surface shear strain rate at x over the interval [0,t], squared, i.e.

$$\bar{e}(t) = \frac{\Delta e}{\Delta t} \qquad (1)$$

$$e'(t) = \frac{1}{t}\int_0^t \bar{e}(t)dt \tag{2}$$

$$LGC = \left[\frac{\bar{e}(t)}{e'(t)}\right]^2. \tag{3}$$

The LGC can vary over several orders of magnitude, so that values of the quantity _ = $\log_{10}[1 + LGC]$ compare favorably with values of CFF in numerical simulations. Below is shown the correlation between CFF, on the left, and LGC, on the right, for computer simulations of the fault system. The observable LGC is seen to be a close representation of the unobservable CFF. By applying this technique to the actual SCIGN data, it may be possible to not only identify areas of high stress, but to define other such mappings as well. While the theory behind this technique was published this summer (Tiampo et al., *PAGEOPH*, 2004), current research includes analyzing the SCIGN data for this LGC signal.

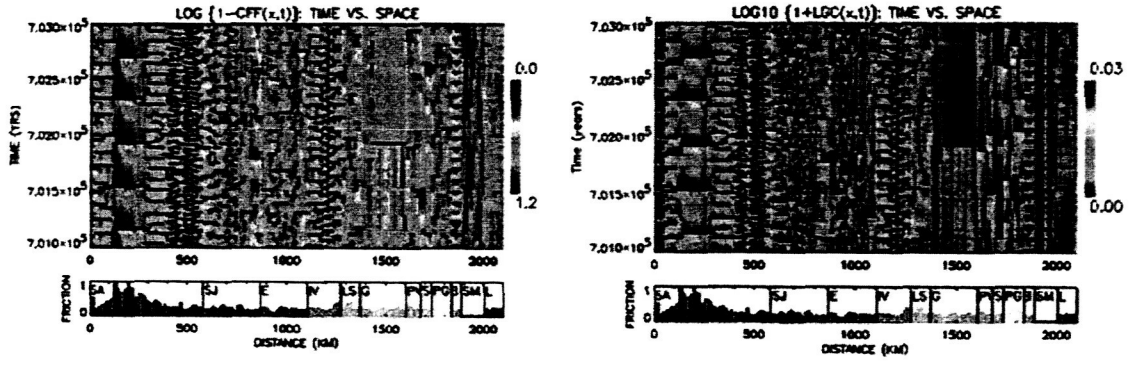

We investigated with numerical simulations the space-time patterns and coherent structures in the data that can be represented as eigenfunctions of an appropriate equal-time correlation operator. These can be used to analyze space-time patterns not only in simulation data, but in deformation and seismicity data as well. With the advances in our capabilities to carry out numerical simulations as illustrated by the figures here, we now have the capability to track changes in deformation and stress through time, and to relate these to the development of space-time correlations and patterns. We therefore have the

capability, for example, to compute eigenfunctions not only for elastic and viscoelastic deformation, but also for Coulomb Failure Functions, Viscoelastic Coulomb Failure Functions, SCIGN data, Interferometric SAR data (InSAR), and historic seismicity data, as well as any other observable of interest that may bear on the causes and mechanisms of deformation and stress within the earth's crust in southern California. Below is shown eigenpatterns from seismicity data for southern California (Tiampo et al., *JGR*, 2002). In short, our methods are perfectly general. As yet, SAR interferometry data has not been shown to possess similar eigenpatterns, but the tantalizing possibility that it does is under active investigation now.

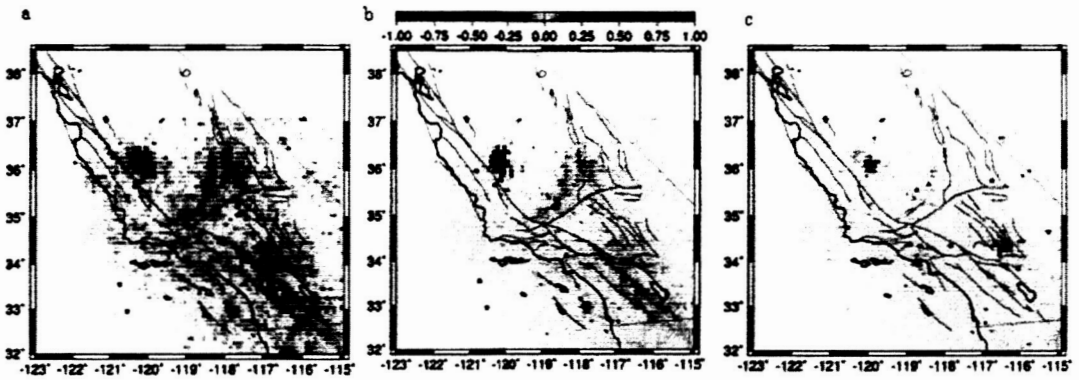

Among our other accomplishments under this project, we analyzed the data for variations in the strain direction. Several modes have a clear pattern corresponding to a surprisingly uniform set of vectors all pointing nearly the same directions horizontally. While the particular character of the horizontal components depends on how the input data are pre-processed, the possibility exists that these changes in the strain direction may be correlated with underlying stress changes associated with pre-, post-, or coseismic signals.

Future work will include the incorporation of KL deformation modes into the appropriate visualizations of these fault simulation programs.

Electrically Actuated Artificial Muscle Composed of a Nematic Liquid Crystalline Elastomer

1. Introduction

The search for "smart materials," which respond to external stimuli (pH variation; ion concentration; temperature; electric field...) by changes in shape or size, has recently attracted considerable attention from the materials research community. In addition to classical approaches such as the shape memory of alloys or ferroelectric polymers (PVF_2),[1] many new materials/approaches are under active investigation, including hydrogels, [2] dielectric elastomers[3] shape memory polymers,[4] conducting polymers; carbon nanotubes, [5] and ferroelectric liquid crystalline elastomers.[6] In addition to the obvious attractiveness of such studies in basic science, artificial muscle systems have many potential applications of great interest for NASA, including serving as the materials foundation for fabrication of sensors, micro-robots, micro-pumps, and actuators with combinations of size, weight, and performance parameters beyond those currently achievable.[7]

Recently, we have developed a new kind of such artificial muscle using side-on nematic liquid crystalline elastomers.[8] This system, based on an idea proposed by de Gennes, [9] makes use of a conformational change of the polymer backbone at the nematic to isotropic phase transition as the motor for a macroscopic contraction.

Although these results are very promising, since we have been able to prepare artificial muscle with mechanical properties approaching those of biological muscle, the main drawback of our approach is the stimulus used, i.e. a temperature jump. It would be much more interesting from various viewpoints to use an electric field as the stimulus for contraction in our side-on nematic liquid crystalline elastomers.

Reported here are the first results obtained in our exploration of an approach to creation of just such electrically actuated LC elastomeric muscle systems.

2. Contraction of a nematic side-on LC elastomer triggered by an electric field

The disorganization of the mesogenic groups in the isotropic phase induces a reduction of the orientational coupling between the mesogens and the polymer backbone, thus inducing a transition from a stretched conformation to a globular conformation for the backbone.

One can assume that application to the oriented nematic side-on LC elastomer of any stimulus which induces to some extent a perturbation in the orientation of the mesogenic groups, also will induce changes in the global organization of the backbones, mimicking the phenomenon happening at the nematic-to-isotropic transition.

In liquid crystal technology, the most often used external stimulus used to induce reorientations of the director in a nematic phase is an electric field. Applying an electric field to a nematic phase composed of molecules with a positive dielectric anisotropy will induce a reorientation of the molecular director (the average long axis of the molecules), which will prefer an orientation parallel to the applied field.

If we now apply an electric field to a nematic side-on elastomer made of mesogenic molecules with strong positive dielectric anisotropy, and oriented with the director perpendicular to the field, we can envisage a similar effect, as indicated below.

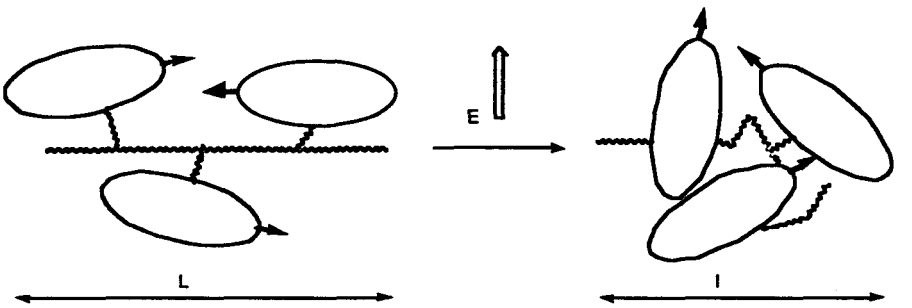

In order for the desired electric field-induced contraction to occur, however, several key factors must be considered, as follows:

- It is possible that such a nematic elastomeric network will be difficult to deform, and will require strong electric fields to overcome the elastic forces resisting macroscopic change in bulk distribution of the material.
- In a related argument, the coupling between the backbone and the mesogenic groups may reduce the freedom of the mesogens, again forcing reliance on a very strong electric field to achieve the desired contraction.

The goals of the present study are twofold: 1) The synthesis of side-on nematic monomers (acrylates and oxiranes) with strong positive dielectric anisotropies, followed by the preparation of aligned side-on nematic elastomers by photopolymerization/photocrosslinking; and 2) Accomplishing initial rheological tests of the new materials to determine if an electric field applied perpendicular to the nematic director of the elastomer can induce a shrinkage of the film along an axis normal to the applied field.

2.1 Synthesis of side-on nematic monomers with large positive dielectric anisotropies

Synthesis of the new materials is based upon the well-established methods we have used to prepare the first generation of side-on nematic acrylate monomers,[8] as shown in Scheme 1. Thus, syntheses of new side-on nematic oxiranes and acrylates have been accomplished, as shown in Schemes 2 and 4, respectively.

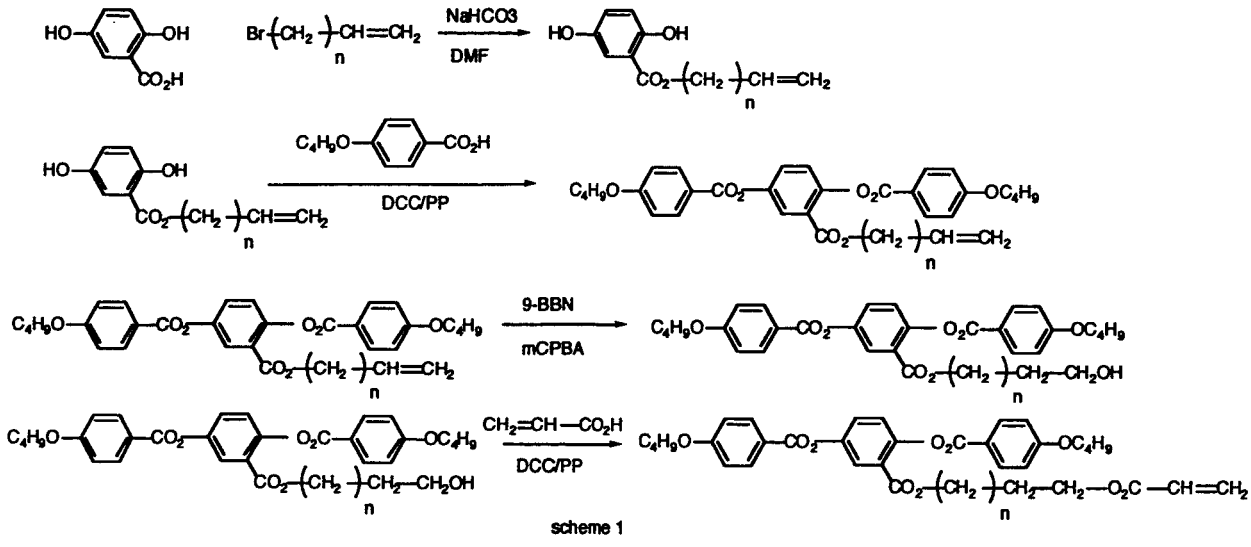

scheme 1

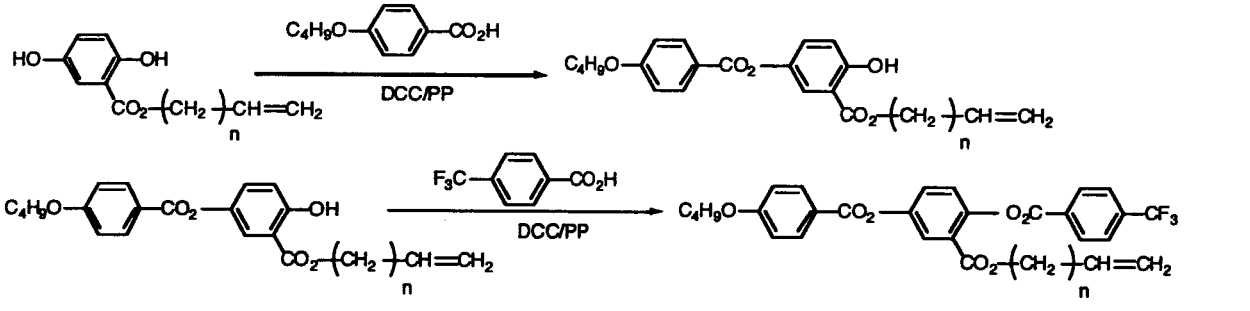

R= -CN; -CF3; -OC4H9

R= -CN; -CF3; -OC4H9

scheme 2

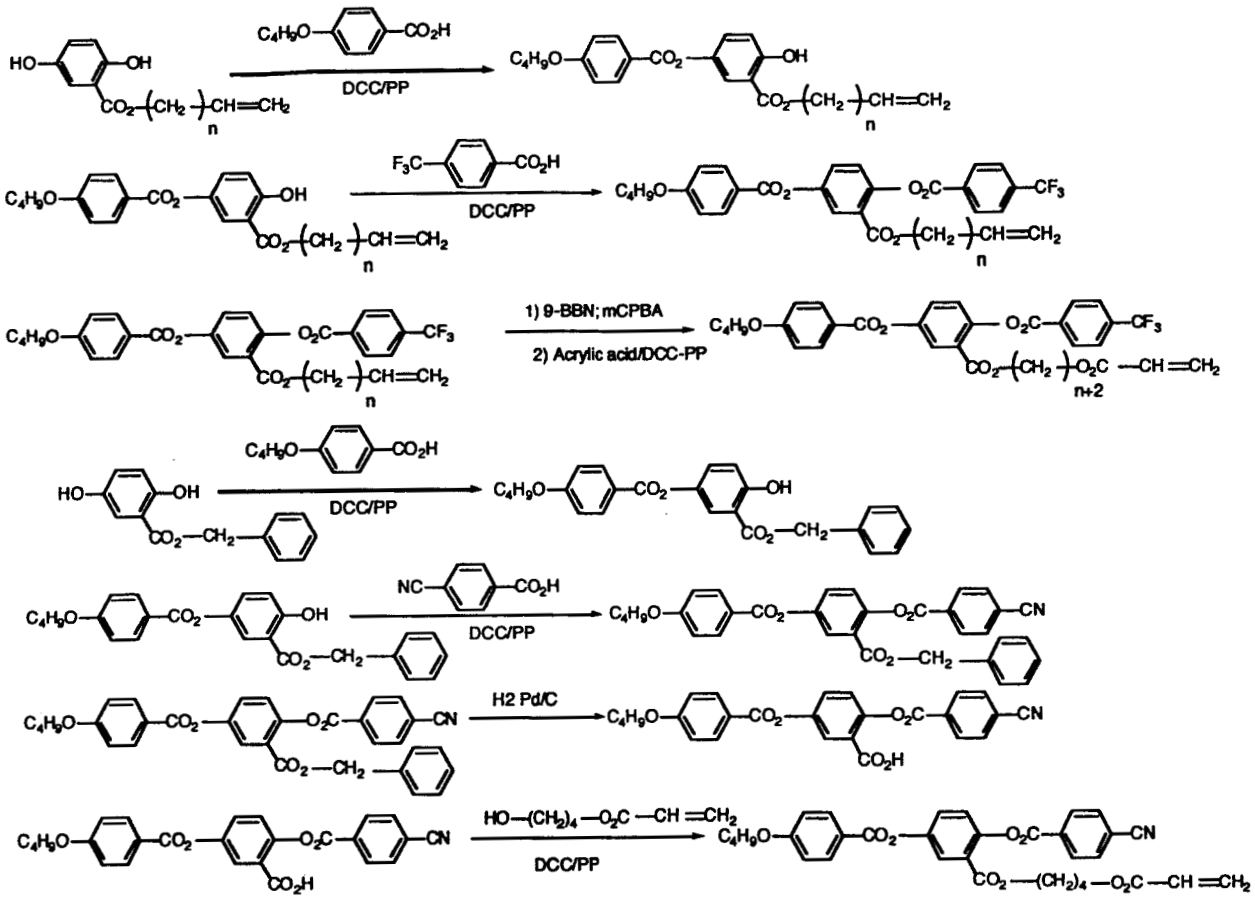

scheme 4

Side-on nematic oxirane monomers

To obtain the required large positive dielectric anisotropies, two different series of compounds, possessing the cyano or trifluoromethyl dipolar groups with dipoles oriented parallel to the director, have been synthesized. It is well known in the liquid crystal literature that similar structures in nematic LCs indeed possess the desired large positive dielectric anisotropy.

We have also synthesized several symmetric (i.e. nonpolar) monomers, which are very easy to prepare. Those monomers have been used in test experiments in order to establish the optimum reaction conditions for the photopolymerization of oxiranes.

The synthetic scheme used (scheme 2) provided easy access to the target compounds.

We studied the mesomorphic properties of the synthesized compounds using optical microscopy and DSC, as reported below.

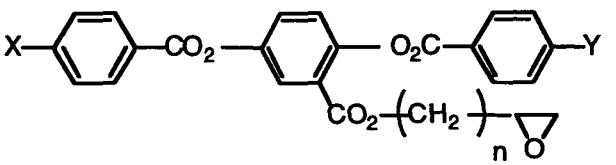

X=	Y=	n=	Phase transition temperatures in °C
OC4H9	CF3	9	K 114 Iso
OC4H9	CN	6	K 69 N 81 Iso
OC4H9	CN	9	K (81 N) 89 Iso
CN	OC4H9	6	K (94 N) 98 Iso
OC4H9	OC4H9	2	K (109 N) 114 Iso
OC4H9	OC4H9	6	K 60.5 N 95 Iso
OC4H9	OC4H9	9	K 66 N 82 Iso
C4H9	C4H9	6	K (28 N) 62 Iso

Most of the new compounds exhibit the expected nematic mesophase, either enantiotropic or monotropic. So, they are suitable for the preparation of the aligned nematic elastomers.

In order to prepare nematic elastomers, a "crosslinking agent" must be added to the monomer sample. In addition to commercially available dioxiranes such as decadiene dioxide (shown in scheme 3), we prepared several new "mesogen-like" crosslinking agents with various numbers of reactive groups (scheme 3). None are mesomorphic, but they should show enhanced miscibility with the monomers. Some of these custom polyepoxides have been used in our attempts to prepare elastomers via photopolymerization.

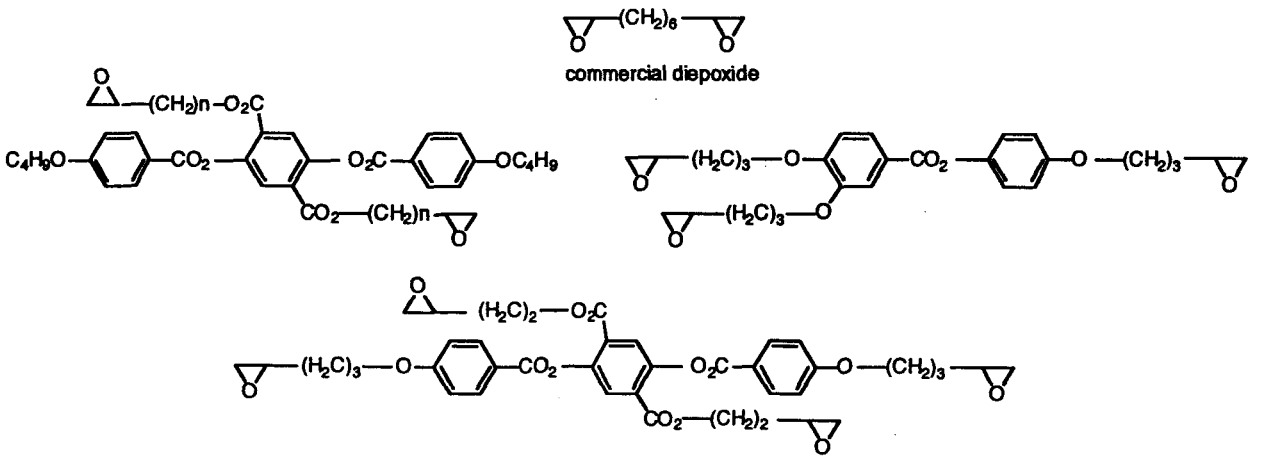

Scheme 3

Side-on nematic acrylate monomers

Nonsymmetrical polar acrylate monomers have been prepared as shown in scheme 4. Depending of the polar group used, -CF_3 or –CN, different routes were applied, taking into account the chemical reactivity of the groups present in each monomer. Compared to the oxirane monomers,

the acrylate monomers are much more difficult to prepare, mainly because they have a strong tendency to polymerize during purification. However, several acrylate monomers were obtained, and their mesomorphic properties studied, as shown below.

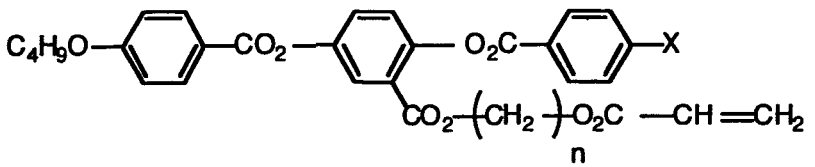

X	n	Phase transition temperature in °C
CN	4	K (72 N) 78 Iso
CF3	6	K (39 N) 77.5 Iso
CF3	8	K 85 Iso
OC4H9	4	K 72 N 98 Iso

We have also prepared mesogen-like custom acrylate crosslinking agents, which can be used in the preparation of the elastomers (scheme 5).

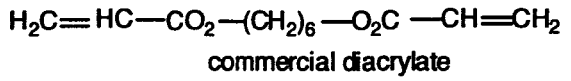

commercial diacrylate

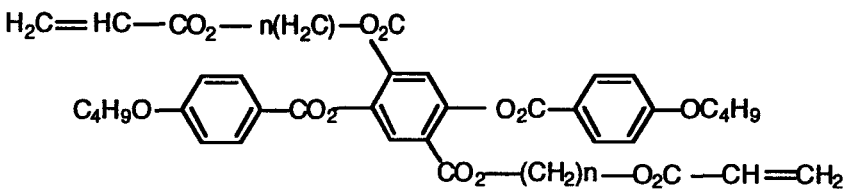

Scheme 5

2.2 Preparation of the side-on nematic elastomers

In order to prepare aligned side-on nematic elastomers, we have used the same basic techniques described previously. Specifically, alignment of the nematic phase of the monomer in LC cells has been achieved using rubbed polyvinyl alcohol. Using a mixture made of one (or several) of the new monomers, a liquid crystalline or liquid crystalline-like difunctional monomer (the crosslinking agent) and a photoinitiator, we tried to induce photochemical polymerization and crosslinking reactions simultaneously in order to freeze in the molecular organization and get well aligned nematic elastomers.

At first, we focused mainly on the preparation of nematic elastomers from oxirane monomers. Most of the commercially available photoinitiators required in the photochemically induced cationic polymerization of oxiranes are only active when irradiated with UV light around 254 nm. Because of the strong absorption of our monomers at this wavelength, we had to prepare a custom photoinitiator, which works with UV light around 360 nm (scheme 6).

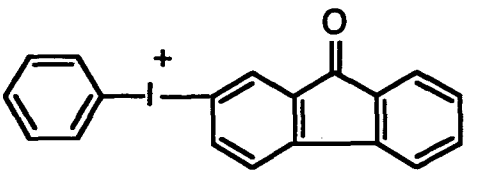

Scheme 6

Using symmetrical non-polar oxirane monomers as a model, we tried to establish suitable conditions for obtaining aligned elastomers. Unfortunately, systematic variations of various parameters (photoinitiator concentration and nature; intensity of light; time and temperature of reaction; functionality of the crosslinking agent; additives (polyalcohols)...), did not provide satisfactory conditions for obtaining aligned elastomers. Although the monomers were consumed in the photopolymerization reactions, no "true" elastomers were formed, only oligomers. The only conditions under which elastomers were obtained required the use of large amounts (40-50 mol %) of tri or tetrafonctionnal crosslinking agents. As suggested by Professor Crivello, side-reactions involving ester groups, which are numerous in our monomers, might produce this surprising and disappointing result. We are still exploring this subject but we are also trying to find new related monomers, which might be more prone to polymerize (see conclusion and perspectives).

We have just begun exploration of the possibility of getting aligned elastomers from polar acrylate monomers. Since none of the polar monomers we prepared have a stable (enantiotropic) nematic mesophase, they are used in mixtures with our "classical" acrylate monomer, which presents a broad nematic mesophase. We have just started to establish a miscibility diagram for these materials. Once a nematic phase containing substantial quantities of the polar mesogens are obtained, we will start the photopolymerization experiments.

2.3 Response of the nematic side-on elastomers to an applied electric field

Since we have not yet succeeded in the preparation of polar side-on nematic elastomers, we have not been able to start this part of the proposal. Once the elastomers are in hand, we will begin a study of the effect of the electric field on the elastomer films visually. In order to see any effect (i.e. contraction) an electric field might have on the elastomer films, soft electrodes which can adjust in size and shape during the evolution in shape and size of the elastomer will be required. We will use compliant electrodes made of conducting grease as describe by Pelrine et al.[3] However, in the first experiments we will use a simpler system in which the elastomer, floating freely in silicon oil, will be placed between two ITO-coated glass microscope slides in a capacitor-kind of geometry.

3. Conclusions

The goal of this research project was to prepare and characterize a new series of side-on nematic LC elastomers in the context of development of electric field-actuated artificial muscles. After the first 3 months, we have obtained two series of new monomers. We are now in the process of preparing the corresponding elastomers. However, since we have encountered difficulties in the photopolymerization of the oxirane monomers, we are exploring new families of monomers,

mainly nematic side-on vinyl-ether monomers such as the ones shown in Scheme 7. Vinyl-ether monomers are known to be more reactive than oxirane monomers, so we are expecting that their photopolymerization will provide aligned elastomers relatively easily. We are also synthesizing more "exotic" monomers (scheme 8), which can be photopolymerized using classical radical photoinitiators.

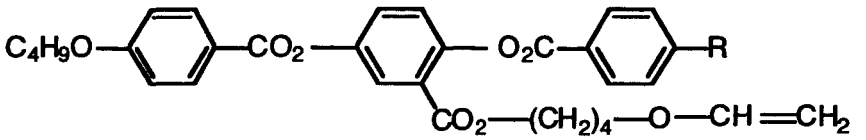

With R = OC4H9, CF3, CN

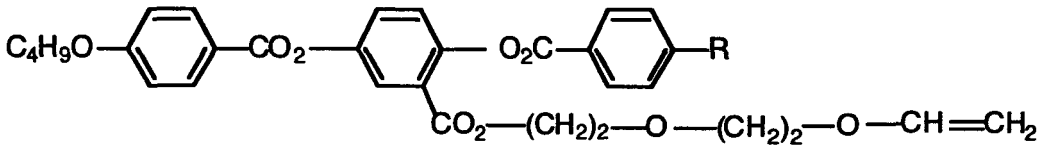

With R = OC4H9, CF3, CN

Scheme 7

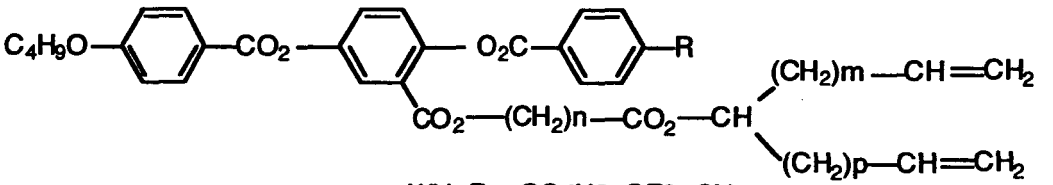

With R = OC4H9, CF3, CN
n = 3, 5,10
m,p = 0
m = 0 p = 1
m = 1 p = 1

Scheme 8

REFERENCES

1 *Electroactive polymer (EAP) actuators as artificial muscles - reality, potential and challenges*; Bar-Cohen, Y., Ed.; SPIE-The International Society for Optical Engineering Vol. PM98, 2001.

2 Liu, Z. S.; Calvert, P. *Adv. Mater.* **2000**, *12*, 288-291.

3 Pelrine, R.; Kornbluh, R.; Pei, Q.; Joseph, J. *Science* **2000**, *287*, 836-839.

4 Lendlein, A.; Schmidt, A. M.; Langer, R. *Proc. Natl. Acad. Sci. USA* **2001**, *98*, 842-847.

[5] Baughman, R. H.; Cui, C.; Zakhidov, A. A.; Iqbal, Z.; Barisci, J. N.; Spinks, G. M.; Wallace, G. G.; Mazzoldi, A.; De Rossi, D.; Rinzler, A. G.; Jaschinski, O.; Roth, S.; Kertesz, M. *Science* **1999**, *284*, 1340-1344.

[6] Lehmann, W.; Skupin, H.; Tolksdorf, C.; Gebhard, E.; Zentel, R.; Kruger, P.; Losche, M.; Kremer, F. *Nature* **2001**, *410*, 447-450.

[7] Ebefors, T.; Mattisson, J. U.; Kalvesten, r.; Stemme, g. *J. Micromech. Microeng.* **2000**, *10*, 337-349.

[8] Thomsen, D. L. I.; Keller, P.; Naciri, J.; Pink, R.; Jeon, H.; Shenoy, D.; Ratna, B. R. *Macromolecules* **2001**, *34*, 5868-5875.

[9] de Gennes, P.-G. *C.R.Acad.Sci.Paris, Ser. II* **1997**, *324*, 343-348.

3. Publications Resulting in Whole or in Part from Grant

K.F. Tiampo, J.B. Rundle, S. McGinnis, and W. Klein, **Karhunen-Loeve Analysis of Southern California SCIGN Data**, AGU abstracts, Spring AGU meeting, 2001.

K.F. Tiampo and J.B. Rundle. **Eigenpattern analysis of geophysical data sets - applications to southern California.** Interface 2002, the 34th Interface Symposium, Geoscience and Remote Sensing. April 2002.

K.F. Tiampo and J.B. Rundle. **Pattern analysis and data assimilation of geophysical data sets.** Third ACES International Meeting, Computational Science, Data Assimilation, and Information Technology for Understanding Earthquake Physics and Dynamics, May 2002.

Tiampo, K.F. **Pattern dynamics analysis of solid earth data sets.** University of Almeria, Spain, December, 2002.

Tiampo, K.F., Rundle, J.B., Gross, S.J., McGinnis, S., and Klein, W. **Eigenpatterns in southern California seismicity,** *Journal of Geophysical Research*, **107**, 2002.

Tiampo, K.F., Rundle, J.B., McGinnis, S., and Klein, W. **Pattern dynamics and forecast methods in seismically active regions,** *Pure and Applied Geophysics*, **159**, 2002.

Tiampo, K.F. **Pattern dynamics analysis of southern California seismicity.** University of Granada, Spain, February, 2003.

Tiampo, K.F., Rundle, J.B., and Klein, W. **A Pattern Informatics Technique Applied to the Study of Southern California Seismicity**, SCEC Annual Meeting, Oxnard, CA, September, 2003.

Tiampo, K.F., Rundle, J.B., Klein, W., Sá Martins, J.S., and Ferguson, C.D. **Ergodic dynamics in a natural threshold system,** *Physical Review Letters,* **91**, 238501, 2003.

Tiampo, K.F., Rundle, J.B., Sá Martins, J., Klein, W., and McGinnis, S. **Methods for evaluation of geodetic data and seismicity developed with numerical simulations: review and applications,** *Pure and Applied Geophysics,* **161**, no. 7, 2004.

Rundle, J.B., Kellogg, L.H., Tiampo, K.F., Klein, W., Rundle, P.B., and Donnellan, A. **Illuminating the relationship between observable data and unobservable dynamics using numerical simulations of a changing earth,** *Pure and Applied Geophysics,* **161**, no. 9, 2004.

Tiampo, K.F., Rundle, J.B., Klein, W., Ben-Zion, Y., and McGinnis, S. **Using eigenpattern analysis to constrain seasonal signals in southern California,** *Pure and Applied Geophysics,* **161**, no. 9, 2004.

Tiampo, K.F., Rundle, J.B., and Klein, W. **Modeling aftershocks of the Northridge earthquake using a Karhunen-Loeve decomposition of SCIGN data,** *GRL*, in preparation, 2004.